frontiers | Frontiers in Materials

TYPE Original Research
PUBLISHED 28 March 2023
DOI 10.3389/fmats.2023.1179502

OPEN ACCESS

EDITED BY
Gokhan Kilic,
Eskişehir Osmangazi University, Türkiye

REVIEWED BY
Mohamed Abdo,
Zagazig University, Egypt
Mohammed Sadeq,
Sinai University, Egypt

*CORRESPONDENCE
Antoaneta Ene,
Antoaneta.Ene@ugal.ro
H.O. Tekin,
tekin765@gmail.com

SPECIALTY SECTION
This article was submitted to Ceramics and Glass,
a section of the journal
Frontiers in Materials

RECEIVED 04 March 2023
ACCEPTED 20 March 2023
PUBLISHED 28 March 2023

CITATION
Deliormanli AM, ALMisned G, Ene A and Tekin HO (2023), Graphene-bioactive glass composites: Structural, Vickers hardness, and gamma-ray attenuation characteristics.
Front. Mater. 10:1179502.
doi: 10.3389/fmats.2023.1179502

Graphene-bioactive glass composites: Structural, Vickers hardness, and gamma-ray attenuation characteristics

Aylin M. Deliormanli[1], Ghada ALMisned[2], Antoaneta Ene[3]* and H.O. Tekin[4,5]*

[1]Department of Metallurgical and Materials Engineering, Manisa Celal Bayar University, Yunusemre, Manisa, Türkiye, [2]Department of Physics, College of Science, Princess Nourah Bint Abdulrahman University, Riyadh, Saudi Arabia, [3]INPOLDE Research Center, Department of Chemistry, Physics, and Environment, Faculty of Sciences and Environment, Dunarea de Jos University of Galati, Galati, Romania, [4]Department of Medical Diagnostic Imaging, College of Health Sciences, University of Sharjah, Sharjah, United Arab Emirates, [5]Faculty of Engineering and Natural Sciences, Computer Engineering Department, Istinye University, Istanbul, Türkiye

Introduction: Graphene-based materials have gained increasing attention for use in radiation attenuation applications. In this study, pristine graphene nanoplatelet-containing (1, 3, 5, and 10 wt%) borate-based bioactive glass composites were prepared.

Methods: Structural properties, Vickers microhardness, and gamma-ray radiation shielding properties of the fabricated composites were examined in detail.

Results and Discussion: Results revealed that the inclusion of the graphene in the glass matrix led to a decrease in the bulk density of the glass-based composites from 2.41 to 2.31 g/cm^3. Similarly, a decrease in Vickers hardness was obtained as the graphene concentration was increased due to a convoluted effect of the non-uniform distribution of graphene nanoplatelets in the bioactive glass matrix and the higher residual porosity. Vickers hardness of the bare and the 10 wt% graphene-containing bioactive glass discs were measured to be 5.03 $\pm$ 0.28 GPa and 1.87 $\pm$ 0.56 GPa, respectively. On the other hand, the incorporation of graphene starting from 3 wt% decreased the crack propagation after indentation which may be attributed to an increase in fracture toughness. In the study, fundamental gamma ray absorption properties of graphene-containing bioactive glasses were examined in the 0.015–15 MeV incident photon energy range. For this purpose, the Py-MLBUF code was employed to determine gamma ray absorption parameters. Results showed that linear attenuation coefficients of the glass-based composites decreased due to a decrease in the density of the samples. On the other hand, as graphene was incorporated into the bioactive glass structure, exposure buildup factor and energy absorption buildup factor values increased. The growing graphene ratio in the glass structure contributed negatively to the photon's tendency to interact with the material.

KEYWORDS

graphene, bioactive glass, hardness, radiation shielding, Vicker hardness

1 Introduction

In recent years, bioactive glasses have found utilization in a broad spectrum of disciplines, including the medical field, as is apparent from the scientific literature. Although there are several factors that contribute to this increase in popularity, one of the most significant is the developments in bone tissue applications. In addition to restorative materials in dental applications and bone regeneration, bioactive glasses have made it possible to construct biological habitats that behave like bone (Gerhardt and Boccaccini, 2010; Jones, 2013; Hench Larry and Jones Julian, 2015; Rahaman, Day, Bal, Fu, Jung, Bonewald, Tomsia). Recently, the FDA (Federal Drug Administration) has approved an expanding number of bioactive applications, which has led to a significant growth in this frequency of recognition. Identifying a material as bioactive glass is possible if it fulfills certain conditions and standards. According to their chemical structure, the properties of these bioactive glasses may change. In this respect, bioactive glasses have motivated many researchers by pushing the improvement of certain properties and bringing them to more advantageous levels, as well as their internal body applications. The rate of cell growth in bioactive glasses, for example, has prompted the creation of more favorable properties for tissue regeneration processes, particularly *via* the advancement of bioactive glass research in hard and soft tissue engineering (Rahaman, Day, Bal, Fu, Jung, Bonewald, Tomsia). On the other hand, the mechanical properties of bioactive glasses have offered impetus for the creation of internal body durability and behavioral changes that may occur without detriment when exposed to external forces. Various studies on enhancing cell attachment, biocompatibility, and other characteristics of a biological environment are also common in scientific literature (Kaur et al., 2019; Pantulap et al., 2022). Further investigation may be necessary to determine if the chemical compositions added to bioactive glass enhance or subtract from these features. Apart from biocompatibility, recent studies (Deliormanlı et al., 2021a; Al-Harbi et al., 2021; Deliormanlı et al., 2022) have primarily focused on the ionizing radiation absorption capabilities of bioactive glasses as a function of bioactive context. In the aforementioned application areas, these glasses may be subjected to external therapeutic or diagnostic radiation. During this exposure, the interaction mechanism with external radiation or the absorption qualities of glasses that are concentrated inside the body may have a significant impact on the effectiveness of diagnostic or therapeutic radiation therapies. This situation may also be seen from a wider viewpoint. For instance, the increased radiation absorption characteristics that will be added to glasses with high bioactivity may enable vital organs and tissues to play a protective role during radiation treatment or diagnostic procedures. Such a preventive strategy may be especially useful for successful treatment planning, that is one of the most fundamental study objectives in radiation therapy, with the primary purpose of minimizing exposure to healthy tissues while boosting dosage to malignant and cancerous cells. The importance of bioactive glasses in medicinal applications, as well as current scientific literature, prompted us to develop numerous glasses and examine their essential properties. In contrast, graphene-based materials now play a crucial role in the development of novel radiation attenuation materials. Graphene's intense electric conductivity, saturation velocity, exceptional mechanical strength, and optical characteristics make it a potential material for high-performance shielding (Birk and Frank, 2017; Verma et al., 2022). Graphene-containing porous borate-based bioactive glass scaffolds were previously fabricated by the polymer foam replication approach to use in bone tissue engineering applications (Turk and Deliormanlı, 2017). Structural properties, compressive strength, bioactivity, and biocompatibility of the relevant composites have been investigated. According to the findings of the study the use of graphene increased electrical conductivity and enhanced the compressive strength of glass-based composites. The optimal performance was achieved with 5 wt% graphene, which enhanced electrical conductivity with moderate cellular response and *in vitro* hydroxyapatite formation capability. However, ionized radiation shielding characteristics of the graphene-bioactive glass composites were not reported yet. In light of this, dense bioactive glass disc-shaped constructs containing graphene nanoplatelets were fabricated in this study and the Vickers hardness, structural characteristics, and absorption properties of the glass-graphene composites for photons with energy between 0.015 and 15 MeV were investigated in detail. Throughout numerous study stages, the effects of chemical composition alterations on structural, mechanical as well as radiation absorption properties, were fully examined. The current investigation might likewise be seen as a predecessor to scientific investigations that would enhance the conditions and medical usefulness of this form of bioactive glass for individuals.

2 Materials and methods

2.1 Materials

In the study borate-based 13-93B3 bioactive glass (5.5Na_2O, 11.1K_2O, 4.6MgO, 18.5CaO, 3.7P_2O_5, and 56.6B_2O_3 wt%) powders (d_{50}:~3 μm, ρ:2.46 g/cm^3) synthesized by the melt-quench method. Graphene nano powders were obtained from Graphene Supermarket (AO-4 grade, 98.5%, United States). The flake thickness and the particle size were reported to be 60 nm and 3-7 μm by the manufacturer company.

2.2 Preparation of graphene-containing bioactive glasses

Disc-shaped composites of 13-93B3 bioactive glass including graphene nanoplatelets were fabricated using the standard die-pressing technique. Dry mixtures of graphene nanopowders (1, 3, 5, and wt%) and 13-93B3 bioactive glass powders were developed for this purpose. A 1 g powder combination was pressed into a disc-shaped sample using a die made of stainless steel and a hydraulic press under 100 MPa of pressure. For densification, the obtained dis-shape bioactive glass green structures were sintered at 575°C for 1 h (5°C/min heating rate) in an air environment. Table 1 shows the elemental compositions as well as sample codes of the investigated bioactive glass samples.

TABLE 1 Composition of the studied bioactive glass samples.

Sample code	wt%						
	Na_2O	K_2O	MgO	CaO	P_2O_5	B_2O_3	Graphene
B3	5.5	11.1	4.6	18.5	3.7	56.6	0
1G–B3	5.445	10.989	4.554	18.315	3.663	56.034	1
3G–B3	5.335	10.767	4.462	17.945	3.589	54.902	3
5G–B3	5.225	10.545	4.37	17.575	3.515	53.77	5
10G-B3	4.95	9.99	4.14	16.65	3.33	50.94	10

2.3 Structural and mechanical properties

Using a scanning electron microscope, the morphological characteristics of the bioactive glass and graphene nano particles were determined (ZEISS, GeminiSEM 560, Germany). CuKα radiation was used with an x-ray diffraction diffractometer (XRD, Philips XPert, Pro, Netherlands) to examine crystallinity. We used FTIR spectrometer (Thermo Scientific-Nicolet IS20, United States) with an ATR attachment in terms of determining the chemical bonds of produced bioactive glass samples. Archimedes' liquid displacement technique was used to calculate the bulk densities of the graphene-containing bioactive glass discs (10 mm in diameter and 3 mm in thickness). Throughout the measurements, ethanol was employed as a solvent. Using a microhardness testing equipment (Future-Tech FM-700), measurements of Vickers hardness were taken by applying 100, 300, and 500 g of force for 10 s. Before measuring Vickers microhardness, surfaces of the investigated bioactive samples were polished and wet-ground using 600-grit SiC abrasive paper and ethanol. Each sample was subjected to five hardness tests, and the results were averaged. The Vickers hardness was determined by dividing the kilogram-force load by the indentation's square millimeter area. After indentation, the surface of the glass was studied using a stereo microscope (Nikon SMZ 1000, Japan).

2.4 Gamma-ray attenuation properties

In another crucial phase of the study, the absorption capabilities of the bioactive glass samples against ionizing gamma rays were theoretically investigated across a broad energy range. Absorption coefficients and half-value thicknesses were investigated in the energy range of 0.015–15 MeV for the investigated parameters. These obtained critical absorption values were computed using the Py-MLBUF (Mann and Mann, 2021) software and shown using the ORIGIN2018 software. In this work, exposure, and energy absorption buildup factors in the range of 0.015–15 MeV were estimated and compared for each sample for 0.5 to 40 mfp values. The significant gamma-ray absorption characteristics investigated in this research may be derived from our previously published studies (ALMisned et al., 2022; Kilic et al., 2022; Ozen Ilik et al., 2022) and related studies (Akkurt, 2009; Boodaghi MalidarreAkkurtGunoglu and Akyıldırım, 2021; Bekir, 2022; Sarihan, 2022).

3 Results and discussions

3.1 Structural and mechanical properties

Figures 1A, B shows the SEM micrographs of the starting bioactive glass particles and the as-received graphene nanoplatelets, respectively utilized in the study. Melt-derived borate bioactive glass particles have an irregular morphology whereas graphene nano powders have a two-dimensional flake-like structure. Functional groups in the as-received graphene nano powders and the sintered bioactive glass-based composites were analyzed using FTIR spectroscopy (Figure 2). Accordingly, there are no significant peaks in the FTIR spectrum of pristine graphene due to a lack of functional groups. However, some low-intensity bands are observed at 599 cm^{-1} (C-H bending vibrations), 673 cm^{-1} (C-H bending vibrations), 869 cm^{-1} (C-H bending vibrations), 1,051 cm^{-1} (C–O stretching vibrations), 1,670 cm^{-1} (C=C stretching vibrations), 1,990 cm^{-1} (CH_2 bending), 2,113 cm^{-1} (C=C stretching) (Güler et al., 2015; Hayyan et al., 2015; Surekha et al., 2020). The large absorption-bands at 710 cm^{-1} and 1,350 cm^{-1} in the bending vibrations of BO_3 triangles and the stretching vibrations of BO3 units are likely responsible for the differences in FTIR spectra between the bare and graphene-containing bioactive glass samples. A similar explanation was proposed for the 950 cm-1 band, which was linked to the stretching vibrations of BO_4 units (Deliormanlı et al., 2021b; Kermani et al., 2022). Additionally, in the glass-based composites as the pristine graphene concentration was increased an increase in peak intensities was observed at 599 cm^{-1} which was assigned to the C-H bending vibrations. Figure 2 also demonstrates the XRD pattern of the bare and the graphene-containing (10 wt%) bioactive glass samples. Accordingly, bare glass constructs were amorphous after sintering performed at 575°C, and the XRD pattern of the graphene-containing (at highest concentration) glass samples contains C (002) an intense peak at ~26.5° (2θ). It has been reported that pristine graphene exhibits a basal reflection (002) sharp peak at 27.0° assigned to a d spacing of 3.370 Å in graphite layer structure (Batakliev et al., 2019). The bulk density values of the glass constructs and the Vickers hardness measurement results are given in Figure 3; Table 2. The density of the bare bioactive glass discs was measured to be 2.41 g/cm^3 whereas the density of the 10 wt% graphene-containing glass samples was 2.31 g/cm^3. The decrease obtained in the bulk density of the prepared glass-based composites may be attributed to the lower density of graphene (2.26 g/cm^3) (Yehia et al., 2022) and the presence of some porosity in the disc shape glass samples. Vickers

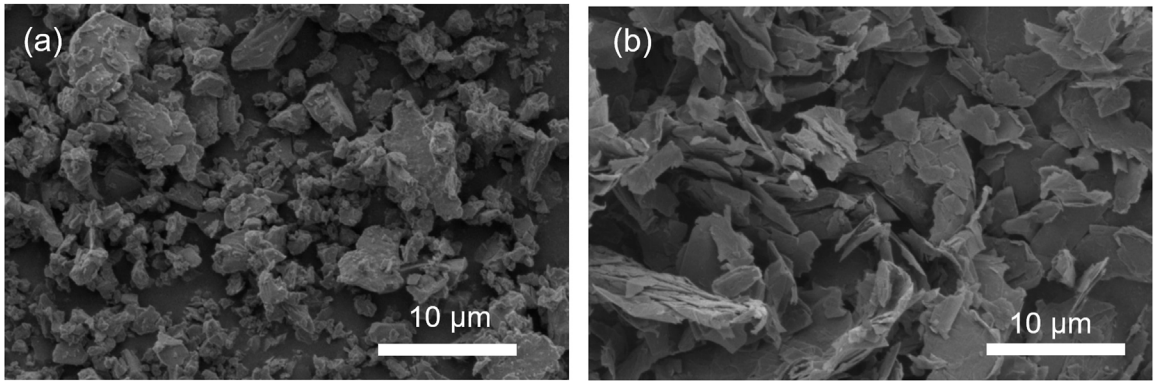

FIGURE 1
SEM micrographs of the **(A)** bioactive glass and the **(B)** graphene nanoplatelets utilized in the study.

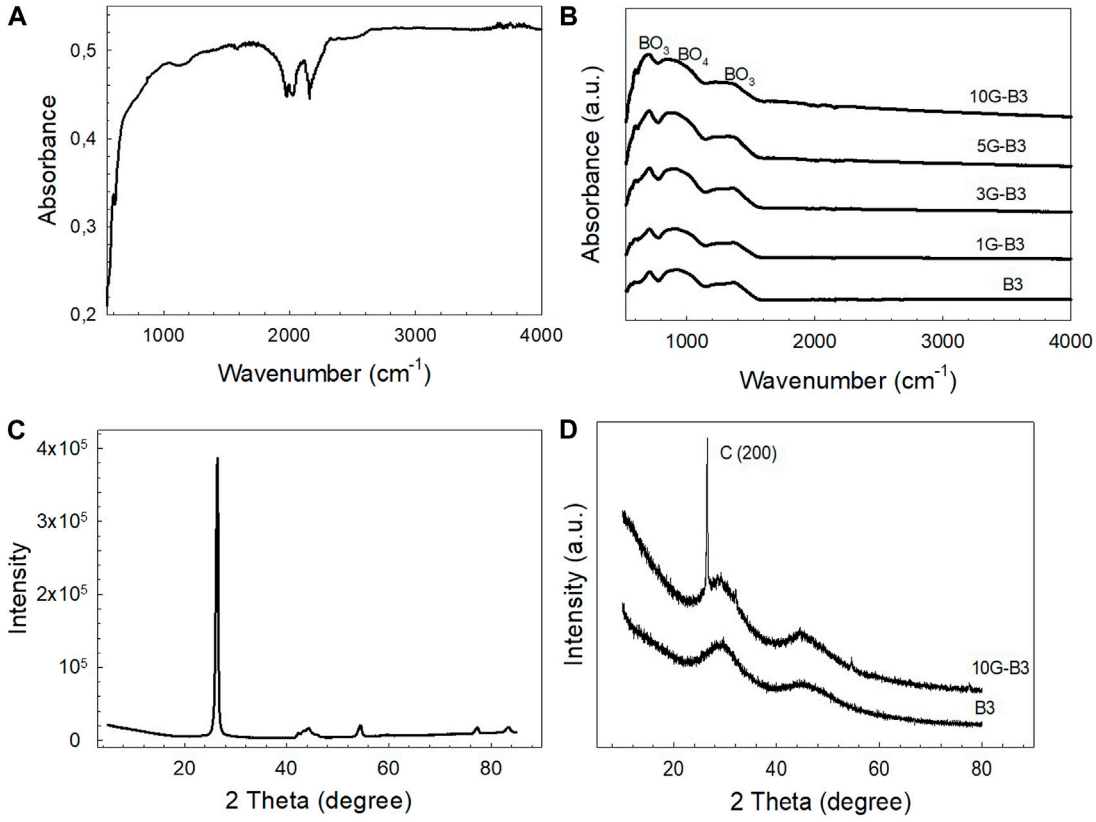

FIGURE 2
FTIR spectra of the **(A)** pristine graphene, **(B)** graphene-bioactive glass composites; XRD pattern of the **(C)** pristine graphene, **(D)** bare glass and the graphene-glass composite after sintering.

microhardness test results are shown in Figure 3B revealing that the Vickers hardness number of the bare bioactive glass discs was 513.10 ± 29.5 (5.03 ± 0.28 GPa). On the other hand, for the graphene-containing glass samples, a decrease in hardness values was obtained. Accordingly, the Vickers hardness number of the 10 wt% graphene-containing glass sample was measured to be 191.5 ± 58.6 (1.87 ± 0.56 GPa). The significant reduction obtained in Vickers hardness values as the graphene concentration was increased may be due to a convoluted effect of the non-uniform distribution of graphene nanoplatelets in the bioactive glass matrix and the higher residual porosity. It is also important to note that, the presence of graphene nanoplatelets in the bioactive glass matrix at less than 1 wt% may cause a different effect on the mechanical properties due to the lower possibility of agglomeration inside

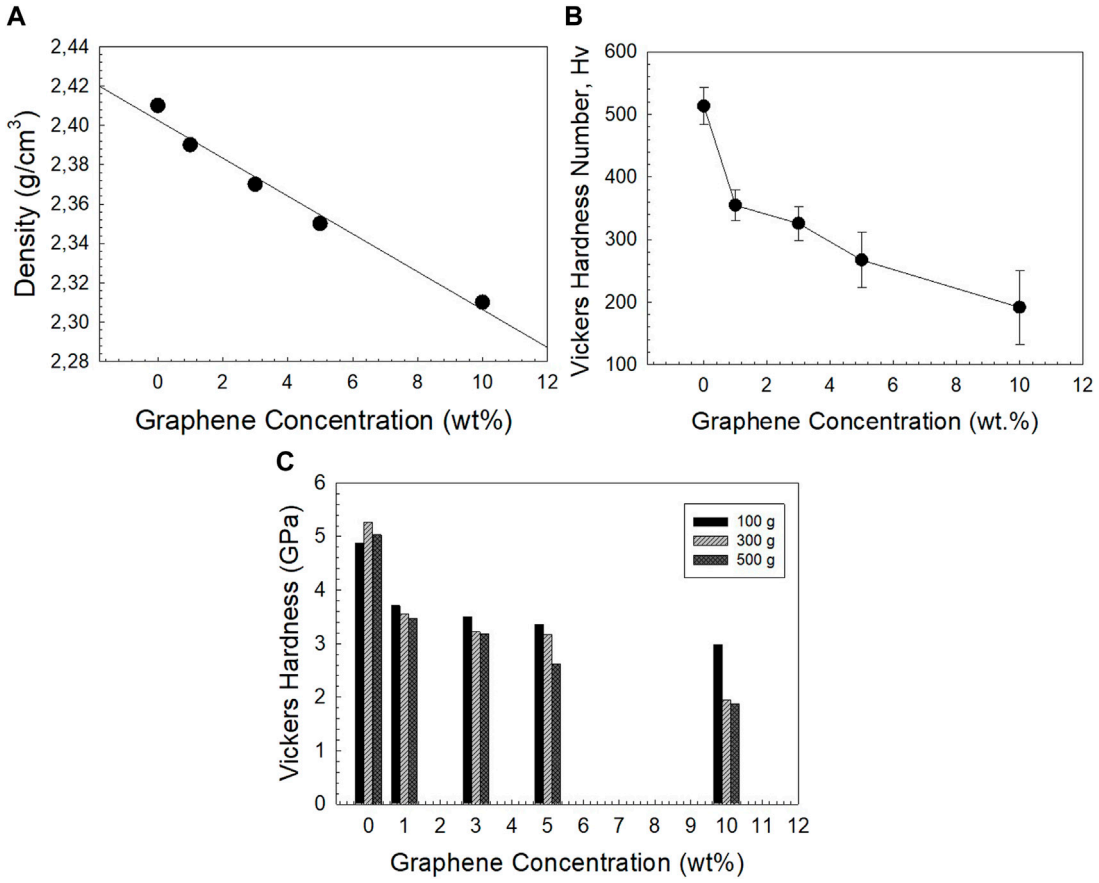

FIGURE 3
Graphs showing the **(A)** bulk density values of the samples measured by the Archimeds method, **(B)** Vickers hardness numbers of the glass samples measured at 500 g, **(C)** Vickers hardness values at different loads.

the glass matrix. Using nanoindentation, nanoscratch, and the Vickers indentation test, Gu et al. (2022) studied the effect of graphene on the indentation and scratch properties of soda lime silicate glass. To do this, a monolayer graphene coating was CVD-applied on the surface of the glass. The findings indicated that the nano hardness, Vickers hardness, and decreased modulus of graphene-coated glass were all greater than those of bare soda lime silica glass. This is because the graphene-coated glass surface can tolerate more strain energy *via* the elastic process. Ilyas et al. (Kanwal IlyasZahid et al., 2019) reported the preparation of graphene oxide-bioactive glass-ceramic composites. An increase in microhardness was obtained with the addition of graphene oxide up to 1 wt%, in contrast, further loading caused a decrease in hardness. The increase obtained in hardness was attributed to the better interlocking between glass and graphene oxide, which is directly bonded by attractive electrostatic forces. Results of the current study also revealed that as the indentation load was increased from 100 to 500 g a decrease was obtained in Vickers hardness values (Figure 3C; Table 2). The obtained decrease in hardness values as a function of applied indentation load was especially significant for the glass samples containing graphene at the highest concentration. Microhardness of solids is reported to change with the indentation load used. The perceived microhardness often decreases with increasing applied force (save for extremely tiny indentation loads), a phenomenon known as the indentation size effect (Petrík and Palfy, 2011). This effect may be evaluated using Meyer's Law. Vibration and indenter bluntness at low loads, applied energy loss from specimen chipping around the indentation, and development of median or radial fractures during the indenter loading half-cycle (Gong et al., 1999; Petrík and Palfy, 2011) all contribute to this disparity. Figure 4 demonstrates the optical microscope images of the indentation crack paths on the surface of the bare and the graphene-containing (1 and 10 wt%) 13-93B3 glass samples. Accordingly, the formation of radial cracks is observed clearly in the bare bioactive glass sample however, in the case of 10 wt% graphene-bioactive composite samples the absence of crack propagation may be taken as the indication of the toughening. The presence of cracks along the diagonals for the bare B3 as well as the 1G-B3 glass sample suggests that the sample behaves in a brittle manner. However, crack paths were not detectable for samples containing graphene starting from 3 wt% (results not shown). Although fracture toughness of the bare and graphene nanoplatelet-containing glass samples was not calculated in the study, an increase in toughness may be expected up to a specified graphene concentration for the composite samples. Previously, Bozkurt et al. (2021) investigated the influence of pristine

TABLE 2 Vickers hardness numbers (at different indentation loads) and the bulk densities of the bare and graphene-containing bioactive glass samples.

HVN	0% G-B3	1% G-B3	3% G-B3	5% G-B3	10% G-B3
F = 100 g	498.6 ± 37.7	378.6 ± 23.5	357.63 ± 55.8	343.56 ± 40.1	304.73 ± 41.4
F = 300 g	537.40 ± 35.6	362.26 ± 35.3	329.1 ± 36.1	323.15 ± 48.2	199.36 ± 62.4
F = 500 g	513.10 ± 29.5	354.46 ± 24.5	325.6 ± 26.7	267.2 ± 44.1	191.5 ± 58.6
ρ (g/cm^3)	2.41	2.39	2.35	2.32	2.29

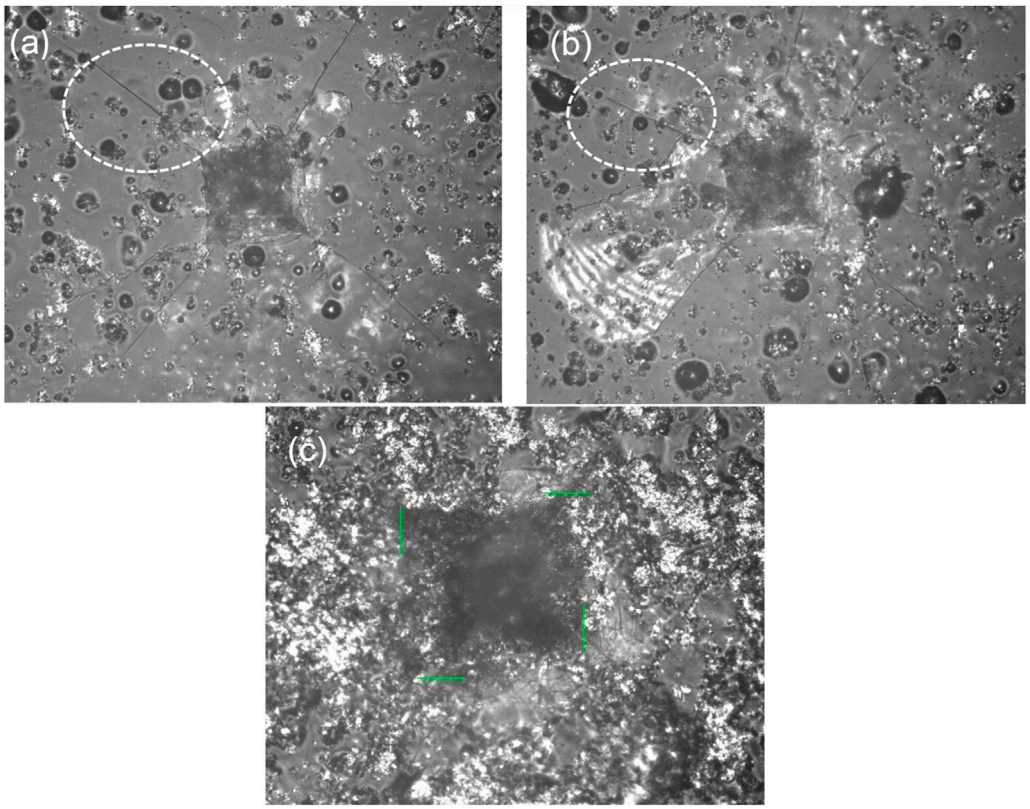

FIGURE 4
Optical microscope images showing the diagonals of the indentation left in the surface of the **(A)** B3, **(B)** 1G-B3, and **(C)** 10G-B3 bioactive glass samples after removal of the 500 g load; Magnification ×20.

graphene nanoplatelets (up to 2 vol%) on the Vickers hardness and the fracture toughness of hydroxyapatite (HA) and Si3N4 ceramics. 18% decrease was observed in the Vickers hardness of the Si3N4-HA-graphene composites with increasing graphene concentration. On the other hand, an improvement was obtained in the fracture toughness and it was attributed to pull-out and crack deflection mechanisms. It has been reported that the presence of crystalline phases in the matrix enhances the strength of glass or glass-ceramics and led to an increase in fracture toughness when compared to the parent glass. In this context, crack bridging and crack deflection are the most potent toughening mechanisms (Apel et al., 2008; Kaur et al., 2019). Toughening observed in the current study for the graphene-glass composites can be explained by the same mechanisms.

3.2 Gamma-ray attenuation properties

In addition to the structural and mechanical properties of graphene-containing bioactive glasses, their absorption properties against photons with energies between 0.015 and 15 MeV are also examined in this work. Initially, the linear attenuation coefficients of bioactive glasses were determined, and their attitude in the low, medium, and high energy regions was addressed as a function of increasing photon energy. Changes in the linear attenuation coefficients of the investigated bioactive glasses are shown in Figure 5. The linear attenuation coefficient is a density-dependent coefficient that is quantifiable for each mono-energy value. This parameter represents the proportion of monoenergetic primary photons attenuated per unit thickness of the material and is represented in

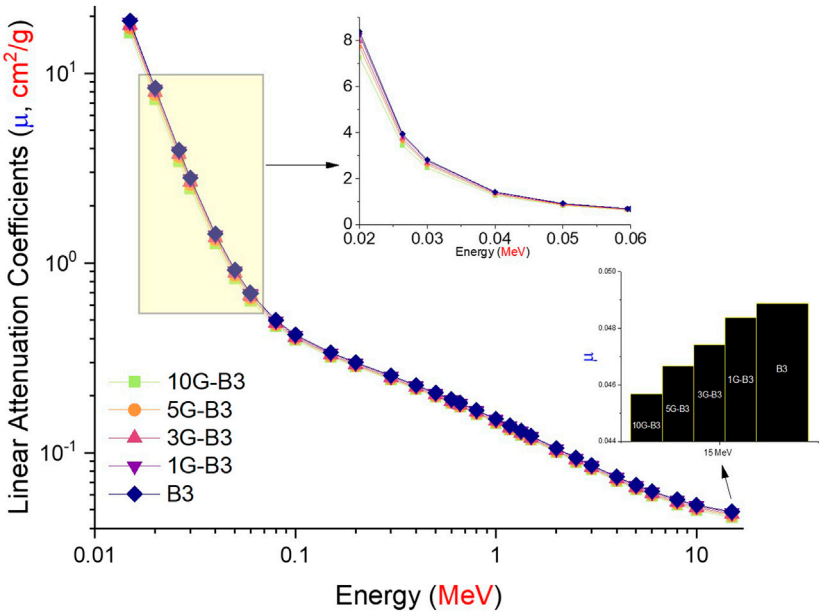

FIGURE 5
Variation of linear attenuation coefficient (cm^{-1}) with photon energy (MeV) for all 10G-B3 to B3 glasses.

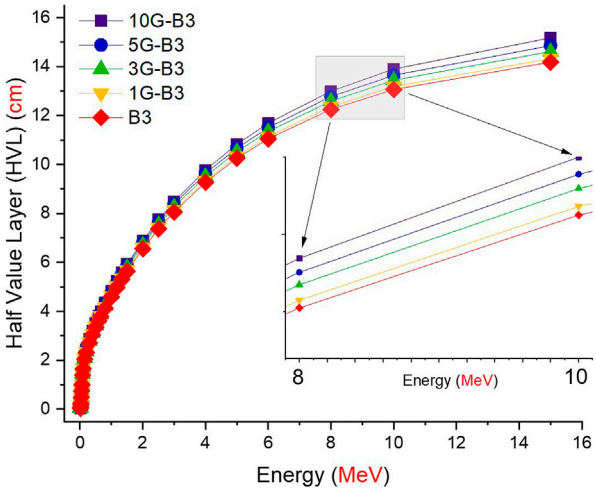

FIGURE 6
Variation of half value layer (cm) with photon energy (MeV) for all 10G-B3 to B3 glasses.

cm^2/g. As seen in the graph, the μ values in the low energy region are the highest for each glass sample. This is because the material effectively absorbs low-energy primary photons per unit thickness. Under the photoelectric effect, photons of low energy and, thus, limited penetration are quickly absorbed in the low energy region. This is a crucial indicator of potential attitudes of photon-matter interactions as a function of incident photon energy level. The increase in energy led to a significant decrease in μ values. This may be due to the increase in the penetrating strength of primary photons during the shift from the low-energy to the middle-energy region, as well as the switch in the dominating photon-matter interaction from the photoelectric effect to Compton scattering. In other words, based on the increase in energy, the primary photon might also eject an electron from its orbit or conduct secondary and sequential scattering with the remaining energy. This process continues until the initial photon passes through the material in a scattered state or is fully absorbed due to scattering and interactions inside the material. In contrast, μ values have achieved their lowest level in the high-energy region. This means that a smaller percentage of high-energy photons are absorbed per unit thickness of the material. Although comparable trends are found for all examined bioactive glasses, the B3 sample without graphene in its structure has the highest μ values for each energy value. The addition of graphene to the B3 sample is likewise seen to generate a regular decrease in the μ values of the materials. It has been found that 1, 3, 5, and 10 wt% graphene, which contributes to B3, also reduces the μ values in a systematic manner. This may be explained by the fact that incorporation of graphene to the bioactive glass matrix at concentrations ranging from 1% to 10% reduces the bulk density of the composites. Previous studies of Sayyed et al. showed that incorporation of the high-density compounds such as PbO (Sayyed et al., 2023), Fe_2O_3 (Sayyed et al., 2022a), Y_2O_3 (Sayyed et al., 2022b), and AgI (Sayyed et al., 2022c) to the glass systems having varying compositions caused a significant increase in the radiation shielding parameters. As stated previously, the linear attenuation coefficient is a density-dependent parameter; hence, this variation in μ values is due to the inversely proportional dependency of the examined parameter on density value. Nevertheless, even at the maximum energy value, these

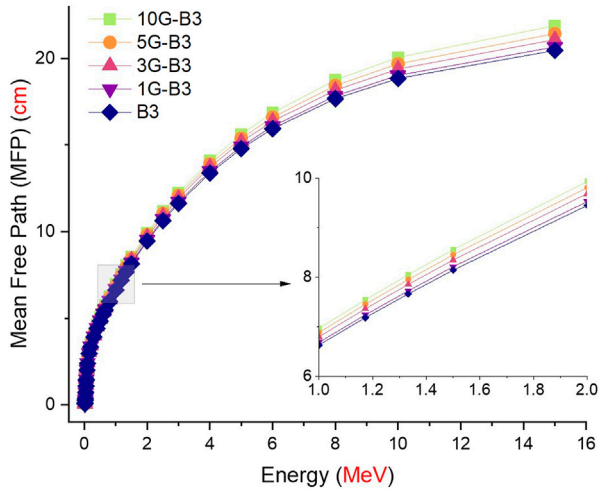

FIGURE 7
Variation of mean free path (cm) with photon energy (MeV) for all 10G-B3 to B3 glasses.

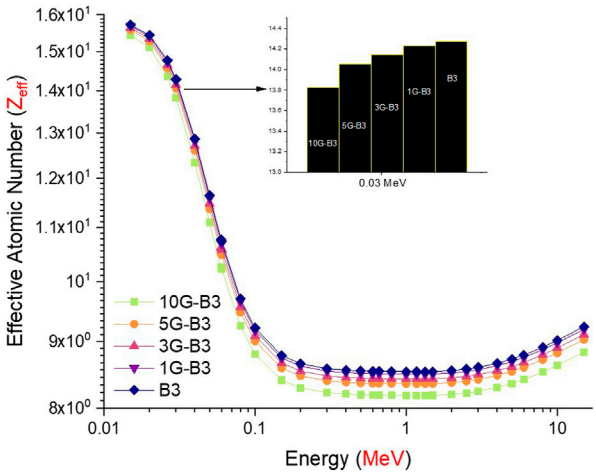

FIGURE 8
Variation of effective atomic number (Z_{eff}) with photon energy (MeV) for all 10G-B3 to B3 glasses.

changes are insignificant. Therefore, while increasing the graphene content from 0% to 10% wt. decreases the μ values, this change is not dramatic. This is also evident from the behavioral changes in the specific energy ranges shown in Figure 5. Half value layer (HVL, cm) is an additional significant quantity that may be determined using the linear attenuation coefficient. This value is the minimum material thickness required to reduce the number of primary photons by half and is inversely related to the linear attenuation coefficient (Omoumi et al., 2021). In other sense, the sample with the maximum linear attenuation coefficient at a single energy value for a given material group would have the lowest HVL value. Similarly, the sample with the lowest linear attenuation coefficient would have the highest HVL value. A crucial indicator of outstanding absorption properties is a high linear attenuation coefficient. The fact that this circumstance results in low HVL values is also a crucial indication that may be attributed to its better absorption capabilities; it demonstrates that the density of a photon with a certain energy can be halved at thinner material thicknesses (Chang et al., 2014). In other words, the halving of a photon with the same energy at thinner layers is a consequence of its improved absorption properties. Figure 6 depicts the pattern of change in the HVL values of the investigated bioactive glasses between 0.015 and 15 MeV. As seen in the figure, photons in the low energy region may be halved at low thicknesses. This situation is comparable to the variation in linear attenuation coefficient values. Photons with poor penetration and low energy have suffered a significant fractional mass decrease (Lecoq et al., 2020). From the HVL idea, each bioactive glass sample was sliced at low thicknesses. The needed bioactive glass thickness for quantification rose proportionally to the increase in energy. Consequently, the largest HVL values were attained in maximal energy. Among the investigated bioactive glasses, the B3 sample with zero graphene contribution was reported with the lowest HVL values. Moreover, HVL values increased because of the 1–10 wt% graphene doping added into B3 sample. At each energy level, the 10G-B3 sample with 10% wt. graphene addition exhibits the highest HVL values. This circumstance is also compatible with the minimum linear attenuation coefficient values determined for the 10G-B3 sample. For an energy value of 0.1 MeV, the HVL values calculated for B3, 1G-B3, 3G-B3, 5G-B3, and 10G-B3 were 1.6519, 1.6679, 1.7007, 1.7272, and 1.7614 cm, respectively. As a consequence of the 10 wt% graphene doping, the thickness necessary to reduce the intensity of a mono-energy photon beam with an energy value of 0.1 MeV should be 0.1095 cm thicker. Considering the beneficial effects of graphene doping, this difference may be seen as compensable value for halving the intensity of a photon beam with an energy of 0.1 MeV (i.e., 100 keV), and it is not a substantial difference. Mean free paths are shown to be longer for higher energy photons in the Figure 7. This ties along with the fact that high-energy photons may penetrate deeper, indicating that the photon in the substance under consideration must travel farther before secondary interaction can take place. The mean free path value for the bioactive glass sample B3 was the lowest among all the glasses evaluated. Photons of a given energy would repeatedly collide at close ranges inside the B3 glass. It follows from this that shorter distances would be preferable for the absorption process inside B3 glass. Yet, the research shows that increasing the graphene content of the bioactive glass led to a higher mfp value. This suggests that, depending on the quantity of graphene contained in the bioactive glass composition, consecutive interactions will occur at larger distances. In radiation physics and related subjects, the symbol for the Effective Atomic Number is Z_{eff}. At given time, several other electrons would be trapped between a far-away electron and the nucleus. As a result, the electrons will neutralize some of the nucleus' positive charge, reducing the attractive force between the nucleus and an electron at greater distances. As a consequence, the effective atomic

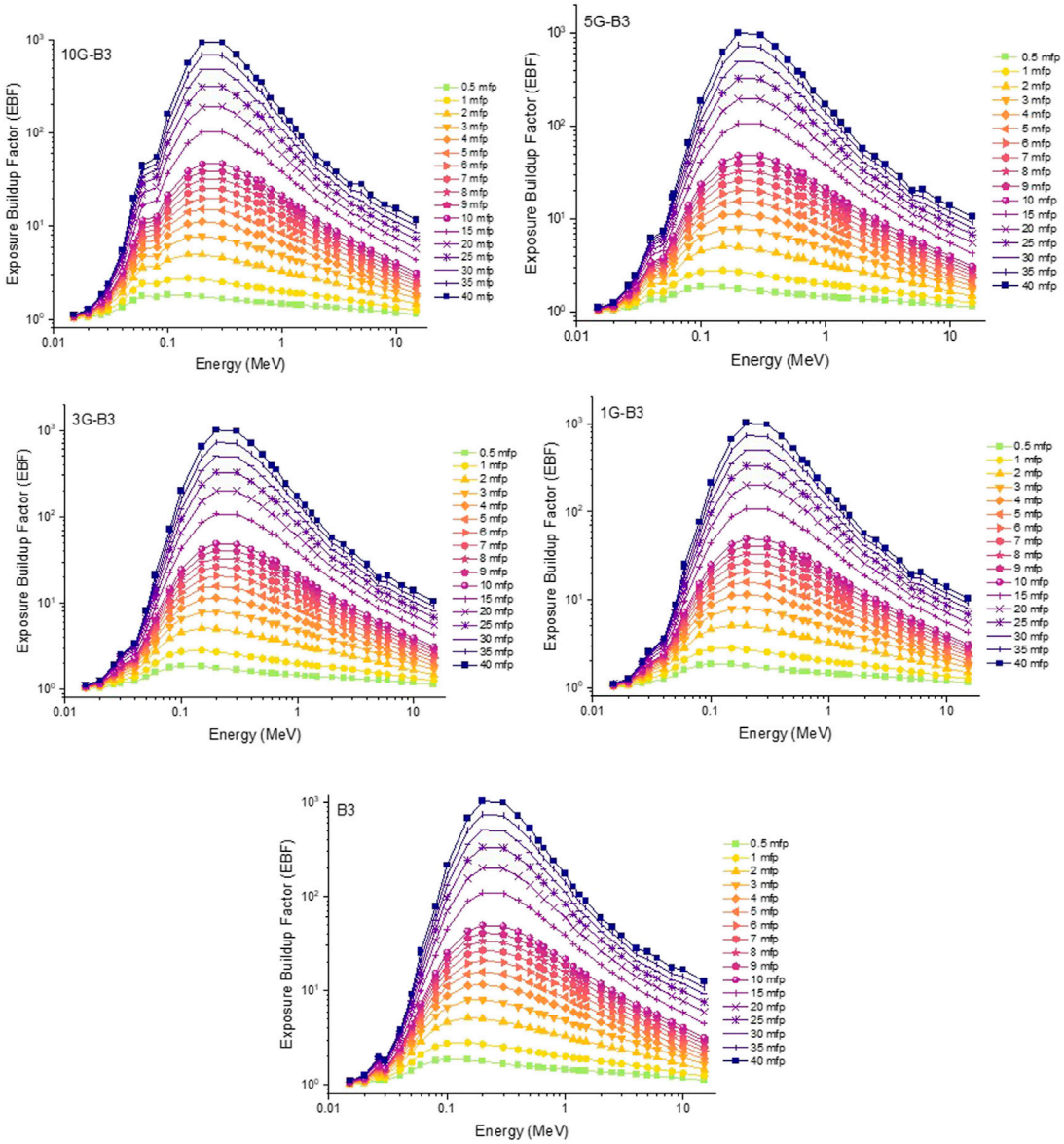

FIGURE 9
Variation of exposure build-up factors (EBF) of investigated glasses at different mean free path values.

number (Z_{eff}) experienced by the electron at a longer distance is smaller than the real nuclear charge (Z). Due to the superiority of high Z_{eff} samples, a sample with a higher Z_{eff} value would play a crucial role in the shielding process. Figure 8 depicts the variation of effective atomic number (Z_{eff}) with photon energy (MeV) for all 10G-B3 to B3 glasses. In all three energy regions, the maximum Z_{eff} values were found for B3. This might be because of dissimilarities in Z values between graphene and the translocated component of bioactive glass sample. Instead, the Z_{eff} value decreased as graphene content increased, resulting in the lowest Z_{eff} values for the highest graphene-contributing 10G-B3 sample. The gamma-ray buildup factor is a useful tool for estimating the radiation's responsiveness to different shielding setups, and it also offers insight into the radiation's behavior in these setups. It is possible to define the gamma ray photon buildup factor as the ratio of the adjusted value of a flux to the un-collided photon flux after transmission through a slabs of a unique optical depth. Generally, in materials with low buildup factor, the ratio of interacting photons is higher than the ratio of non-interacting photons. The increase in the photon-matter interaction, on the other hand, makes a positive contribution to the absorption process, resulting in the complete release of the incident energy in the material as a result of interactions and scatterings. Figures 9, 10 depicts the variation of exposure build-up factors (EBF) and energy absorption buildup factors of investigated bioactive glasses at different mean free path values. At 0.5 mfp, both EBF and EABF values decrease to their minimums, as seen in the figure. This condition demonstrates that the major absorption occurs at the onset of the mfp values, and that there is a large number of

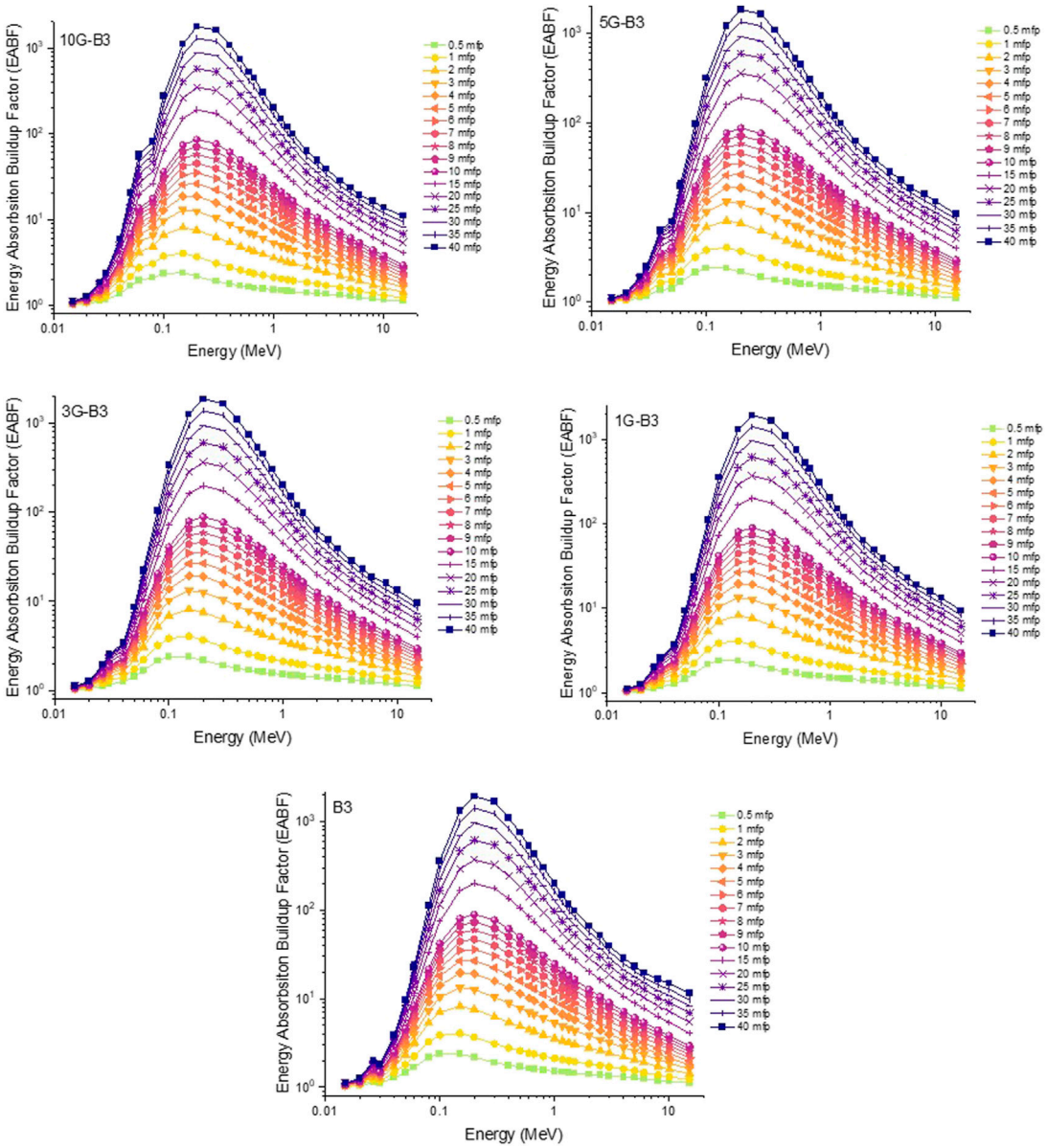

FIGURE 10
Variaton of energy absoption buildup factors (EABF) of investigated glasses at different mean free path values.

interacting photons in the material with an average path of 0.5 mfp. Furthermore, both the EBF and EABF values were rather minimal in the low energy region. This is because of the limited penetrability of the material and high absorption rate of photons with low energy. This is linked to the fact that photons of low energy are rapidly absorbed. Maximum EBF and EABF values were seen in the middle energy area where Compton Scattering is dominant, and these values began to decrease as energy was increased. Due to its higher percentage of photon-matter interaction, B3 was shown to have the lowest EBF and EABF values among all of the bioactive glasses examined. As graphene was incorporated into the bioactive glass structure, EBF and EABF values climbed. The growing graphene ratio in the structure contributes negatively to the photon's tendency to interact with the material, which explains the existing phenomenon.

4 Conclusion

Pristine graphene nanopowder-containing borate-based 13-93B3 bioactive glass disc-shape composites were prepared using die pressing and sintered at 575°C for densification. Structural, mechanical, and ionization radiation shielding characteristics of the fabricated composites were analyzed. Based on the findings of the study, the incorporation of the graphene-nanoplatelets into the glass matrix did not cause crystallization of the glass network. However, an intense C (002) peak was detected in composite

samples due to presence of graphene. The addition of graphene to the glass phase led to a decrease in bulk density and the Vickers microhardness, on the other hand, improved the toughness of the composites. The incorporation of graphene into the bioactive glass composite reduced the gamma absorption characteristics slightly. The linear attenuation coefficients of the glass-based composites decreased due to a decrease in the density of the samples. On the other hand, as graphene was incorporated into the bioactive glass structure, EBF and EABF values increased. The growing graphene ratio in the glass structure contributed negatively to the photon's tendency to interact with the material. The examination of the fundamental gamma ray absorption properties of graphene-containing bioactive glasses in the incident photon energy range of 0.015–15 MeV revealed that the proposed composites have a high potential for use in radiation absorption applications, where critical organs and tissues should be further protected against ionizing radiation during the diagnostic and treatment processes of patients.

Data availability statement

The raw data supporting the conclusion of this article will be made available by the authors, without undue reservation.

Author contributions

AD: Conceptualization, calculations, writing. GA: Calculations, data analysis. AE: Measurements, writing. HT: Writing, calculations, supervision.

Funding

Princess Nourah bint Abdulrahman University Researchers Supporting Project number (PNURSP2023R149), Princess Nourah bint Abdulrahman University, Riyadh, Saudi Arabia.

Acknowledgments

The authors would like to express their deepest gratitude to Princess Nourah bint Abdulrahman University Researchers Supporting Project number (PNURSP2023R149), Princess Nourah bint Abdulrahman University, Riyadh, Saudi Arabia. The author AE would like to thank Dunarea de Jos University of Galati, Romania for material and technical support.

Conflict of interest

The authors declare that the research was conducted in the absence of any commercial or financial relationships that could be construed as a potential conflict of interest.

Publisher's note

All claims expressed in this article are solely those of the authors and do not necessarily represent those of their affiliated organizations, or those of the publisher, the editors and the reviewers. Any product that may be evaluated in this article, or claim that may be made by its manufacturer, is not guaranteed or endorsed by the publisher.

References

Akkurt, Iskender (2009). Effective atomic and electron numbers of some steels at different energies. *Ann. Nucl. En.* 12, 1702–1705. doi:10.1016/j.anucene.2009.09.005

Al-Harbi, Nuha, Al-Hadeethi, Yas, and AhmedBakry, Samir (2021). Mechanical and radiation shielding features of bioactive glasses: SiO2-Na2O-CaO-P2O5-B2O3 for utilization in dental applications. *J. Non-Crystalline Solids* 552, 120489. ISSN 0022-3093. doi:10.1016/j.jnoncrysol.2020.120489

Almisned, Ghada, Sen Baykal, Duygu, Ali, Fatema T., Bilal, Ghaida, and Kilic, G. H. O. (2022). Gadolinium-tungsten-boron trioxide glasses: A multi-phase research on cross-sections, attenuation coefficients, build-up factors and individual transmission factors using mcnpx. *Optik* 272, 170216. doi:10.1016/j.ijleo.2022.170216

Apel, E., Deubener, J., Bernard, A., Holand, M., Muller, R., Kappert, H., et al. (2008). Phenomena and mechanisms of crack propagation in glass-ceramics. *J. Mech. Behav. Biomed. Mat.* 1 (4), 313–325. doi:10.1016/j.jmbbm.2007.11.005

Batakliev, T., Petrova-Doycheva, I., Angelov, V., Georgiev, V., Ivanov, E., Kotsilkova, R., et al. (2019). Effects of graphene nanoplatelets and multiwall carbon nanotubes on the structure and mechanical properties of poly(lactic acid) composites: A comparative study. *Appl. Sci.* 9 (3), 469. doi:10.3390/app9030469

Bekir, Oruncak (2022). Gamma-ray shielding properties of Nd2O3 added iron-boron-phosphate based composites. *Open Chem.* 20 (1), 237–243. doi:10.1515/chem-2022-0143

Birk, A., and Frank, S. (2017). Potential use of graphene as a shielding material in positron emission tomography. *Soc. Nucl. Med.* 58, 1103.

Boodaghi MalidarreAkkurtGunoglu, R. İ. K., and Akyıldırım, H. (2021). Fast neutrons shielding properties for HAP-Fe2O3 composite materials. *Int. J. Comput. Exp. Sci. Eng.* 7 (3), 143–145. doi:10.22399/ijcesen.1012039

Bozkurt, Dilan, Kaplan Akarsu, Melis, Akin, Ipek, and Goller, Gultekin (2021). Phase analysis, mechanical properties and *in vitro* bioactivity of graphene nanoplatelet-reinforced silicon nitride-calcium phosphate composites. *J. Asian Ceram. Soc.* 9 (2), 471–486. doi:10.1080/21870764.2021.1891664

Chang, D. S., Lasley, F. D., Das, I. J., Mendonca, M. S., and Dynlacht, J. R. (2014). "Characteristics of photon beams," in *Basic radiotherapy physics and biology* (New York, NY, USA: Springer). doi:10.1007/978-3-319-06841-1_7

Deliormanlı, A. M., Al-Buriahi, M. S., and Somaily, H. H. (2021). HO tekin,13-93B3 bioactive glasses containing Ce3+, Ga3+ and V5+: Dose rate and gamma radiation characteristic for medical purposes. *Appl. Phys. A* 127 (3), 1–14.

Deliormanlı, A. M., Ensoylu, M., Issa, S. A. M., Rammah, Y. S., Almisned, G., and Ho, Tekin (2022). A thorough examination of gadolinium (III)-containing silicate bioactive glasses: Synthesis, physical, mechanical, elastic and radiation attenuation properties. *Appl. Phys. A* 128 (4), 266–316. doi:10.1007/s00339-022-05408-0

Deliormanlı, Aylin M., Ensoylu, Mertcan, Issa, Shams A. M., Elshami, Wiam, AteyyahAl-Baradi, M. M. S., Al-Buriahi, H. O., et al. (2021). WS2/bioactive glass composites: Fabrication, structural, mechanical and radiation attenuation properties. *Ceram. Int.* 47 (21), 29739–29747. doi:10.1016/j.ceramint.2021.07.146

Gerhardt, L. C., and Boccaccini, A. R. (2010). Bioactive glass and glass-ceramic scaffolds for bone tissue engineering. *Mater. (Basel)* 3 (7), 3867–3910. doi:10.3390/ma3073867

Gong, J., Wu, J., and Guan, Zh. (1999). Examination of the indentation size effect in low-load Vickers hardness testing of ceramics. *J. Eur. Ceram. Soc.* 19, 2625–2631. doi:10.1016/s0955-2219(99)00043-6

Gu, Fenglin, He, Hongtu, Sun, Laixi, Wang, Fang, Zheng, Qiuju, and Yu, Jiaxin (2022). Role of graphene in enhancing indentation and scratch properties of soda lime silicate glass. *J. Non-Crystalline Solids* 597, 121913. doi:10.1016/j.jnoncrysol.2022.121913

Güler, Ömer, Güler, Seval, Selen, Veyis, Albayrak, Muhammet Gokhan, and Evin, Ertan (2015). Production of graphene layer by liquid-phase exfoliation with low sonication power and sonication time from synthesized expanded graphite. *Fullerenes, Nanotub. Carbon Nanostructures* 24, 123–127. doi:10.1080/1536383X.2015.1114472

Hayyan, M., Abo-Hamad, A., AlSaadi, M. A., and Hashim, M. A. (2015). Functionalization of graphene using deep eutectic solvents. *Nanoscale Res. Lett.* 10, 324. doi:10.1186/s11671-015-1004-2

Hench Larry, L., and Jones Julian, R. (2015). Bioactive glasses: Frontiers and challenges. *Front. Bioeng. Biotechnol.* 3, 194. doi:10.3389/fbioe.2015.00194 https://www.frontiersin.org/articles/10.3389/fbioe.2015.00194

Ilyas, Kanwal, Zahid, Saba, Batool, Madeeha, Anwar Chaudhry, Aqif, Jamal, Arshad, Iqbal, Farasat, et al. (2019). *In-vitro* investigation of graphene oxide reinforced bioactive glass ceramics composites. *J. Non-Crystalline Solids* 505, 122–130. doi:10.1016/j.jnoncrysol.2018.10.047

Jones, Julian R. (2013). Review of bioactive glass: From Hench to hybrids. *Acta Biomater.* 9 (1), 4457–4486. doi:10.1016/j.actbio.2012.08.023

Kaur, Gurbinder, Kumar, Vishal, Baino, Francesco, Mauro, John C., Pickrell, Gary, Evans, Iain, et al. (2019). Mechanical properties of bioactive glasses, ceramics, glass-ceramics and composites: State-of-the-art review and future challenges. *Mater. Sci. Eng. C* 104, 109895. doi:10.1016/j.msec.2019.109895

Kermani, F., Sadidi, H., Ahmadabadi, A., Hoseini, S. J., Tavousi, S. H., Rezapanah, A., et al. (2022). Modified sol–gel synthesis of MesoporousBorate bioactive glasses for potential use in wound healing. *Bioengineering* 9, 442. doi:10.3390/bioengineering9090442

Kilic, G., Kavaz, E., Ilik, E., Almisned, Ghada, and Tekin, H. O. (2022). CdO-rich quaternary tellurite glasses for nuclear safety purposes: Synthesis and experimental gamma-ray and neutron radiation assessment of high-density and transparent samples. *Opt. Mater.* 129, 112512. doi:10.1016/j.optmat.2022.112512

Lecoq, P. (2020). "Scintillation detectors for charged particles and photons," in *Particle physics reference library*. Editors C. Fabjan, and H. Schopper (New York, NY, USA: Springer). doi:10.1007/978-3-030-35318-6_3

Mann, Kulwinder Singh, and Mann, Sukhmanjit Singh (2021). Py-MLBUF: Development of an online-platform for gamma-ray shielding calculations and investigations. *Ann. Nucl. Energy* 150, 107845. doi:10.1016/j.anucene.2020.107845

Omoumi, F. H., Wu, X., Ghani, M. U., Wong, M. D., Li, Y., and Liu, H. (2021). Mathematical estimation of half-value layer thicknesses. *J. Appl. Clin. Med. Phys.* 22 (10), 320–328. doi:10.1002/acm2.13385

Ozen Ilik, Buse, Kilic, Gokhan, Ilik, Erkan, Kavaz, Esra, and Ghada Almisned, H. O. (2022). Elucidating the influences of Tantalum (V) oxide in Bi2O3–TeO2–ZnO ternary glasses: An experimental characterization study on optical and nuclear radiation transmission properties of high-density glasses. *Ceram. Int.* 49, 10906–10913. doi:10.1016/j.ceramint.2022.11.284

Pantulap, U., Arango-Ospina, M., and Boccaccini, A. R. (2022). Bioactive glasses incorporating less-common ions to improve biological and physical properties. *J. Mater Sci. Mater Med.* 33, 3. doi:10.1007/s10856-021-06626-3

Petrík, Jozef, and Palfy, Pavol (2011). The influence of the load on the hardness. *Metrol. Meas. Syst.* 18 (2), 223–234. doi:10.2478/v10178-011-0005-5

Rahaman, M. N., Day, D. E., Bal, B. S., Fu, Q., Jung, S. B., Bonewald, L. F., et al. (2011). Bioactive glass in tissue engineering. *Acta Biomater.* 7 (6), 2355–2373. doi:10.1016/j.actbio.2011.03.016

Sarihan, Mucize. (2022). Simulation of gamma-ray shielding properties for materials of medical interest. *Open Chem.* 20 (1), 81–87. doi:10.1515/chem-2021-0118

Sayyed, M. I., Abdo, M. A., Elhosiny Ali, H., Ahmed, H. A., and Sadeq, M. S. (2023). Impact of lead oxide on the structure, optical, and radiation shielding properties of potassium borate glass doped with samarium ions. *Optik* 278, 170738. doi:10.1016/j.ijleo.2023.170738

Sayyed, M. I., Abdo, M. A., Elhosiny Ali, H., and Sadeq, M. S. (2022). Effect of Y2O3 on the structural, optical and radiation shielding properties of transparent Na-rich borate glass with diluted and fixed Fe2O3. *Ceram. Int.* 48 (17), 24310–24318. doi:10.1016/j.ceramint.2022.04.226

Sayyed, M. I., Abdo, M. A., Elhosiny Ali, H., and Sadeq, M. S. (2022). Fe2O3 within Na2O–Al2O3– B2O3 glasses to study the structural and optical features changes. *Opt. Mater.* 131, 112419. doi:10.1016/j.optmat.2022.112419

Sayyed, M. I., Abdo, M. A., Elhosiny Ali, H., and Sadeq, M. S. (2022). Transparent and radiation shielding effective Na2O–CrO3 borate glasses via AgI additives. *Ceram. Int.* 48 (20), 30817–30825. doi:10.1016/j.ceramint.2022.07.035

Surekha, G., Krishnaiah, K. Venkata, Ravi, N., and Suvarna, R. Padma (2020). FTIR, Raman and XRD analysis of graphene oxide films prepared by modified Hummers method. *J. Phys. Conf. Ser.* 1495, doi:10.1088/1742-6596/1495/1/012012

Turk, M., and Deliormanlı, A. M. (2017). Electrically conductive borate-based bioactive glass scaffolds for bone tissue engineering applications. *J. Biomaterials Appl.* 32 (1), 28–39. doi:10.1177/0885328217709608

Verma, Sarika, Sarma, Bibek, Chaturvedi, Kamna, Malvi, Deeksha, and Srivastava, Avanish Kumar (2022). Emerging graphene and carbon nanotube-based carbon composites as radiations shielding materials for X-rays and gamma rays: A review. *Compos. Interfaces* 30, 223–251. doi:10.1080/09276440.2022.2094571

Yehia, H. M., Nouh, F., El-Kady, O. A., Abdelwahed, K., and El-Bitar, T. (2022). Homogeneous dispersion and mechanical performance of aluminum reinforced with high graphene content. *J. Compos. Mater.* 56 (29), 4515–4528. doi:10.1177/00219983221136058